SIMULATION OF THE CO-AXIAL FERROFLUID DROPLETS INTERACTION UNDER UNIFORM MAGNETIC FIELD

by

Atena GHADERI, Mohammad Hassan KAYHANI, and Mohsen NAZARI*

Faculty of Mechanical Engineering, Shahrood University of Technology, Shahrood, Iran

Original scientific paper
https://doi.org/10.2298/TSCI170318158G

In this study, falling and the coalescence of a pair ferrofluid droplets subjected to uniform magnetic field are investigated numerically. For this approach, a 2-D hybrid approach combined of lattice-Boltzmann and finite volume method is used. The lattice Boltzmann equation with the magnetic force term is solved to update the flow field while the magnetic induction equation is solved using finite volume method to calculate the magnetic field. To validate current simulations, three test cases have been considered: Laplace, multiple rising bubbles and deformation of static drop under magnetic field are analyzed. The comparison of results between the present study and previous researches shows a good agreement. The effects of different parameters: magnetic Bond number, magnetic susceptibility, and magnetic field direction are comprehensively studied. The results show that the coalescence of droplets becomes fast with the increasing Bond number and susceptibility in y-direction magnetic field. Also, the coalescence and falling process of droplets takes more time in the horizontal magnetic field in comparison with the vertical magnetic field.

Key words: *lattice Boltzmann method, Shan-Chen model, magnetic field, ferrofluid*

Introduction

The studies of interaction and motion of drops under gravity are of great importance in industrial applications, such as fuel liquid-liquid extraction, emulsification and polymer blending, as well as in natural phenomena like raindrops. Therefore, various researchers have highly focused on this topic and numerous experimental and numerical studies have been performed in this field [1-6].

Numerous techniques can be used for manipulating drops actively, such as: non-uniform temperature field [7], thermocapillarity [8], and electrowetting [9]. Also, applying external magnetic field is an effective and contactless way to control the droplet movement. When a ferrofluid droplet is presented in another fluid with different magnetic properties and they subjected to magnetic fields, the droplet undergoes a shape deformation [10]. This process could significantly influence on the characteristics of droplets. Ferrofluids consist of ferromagnetic nanoparticles coated by a layer of surfactants and suspend in a non-magnetic carrier liquid [10]. Rosensweig [10] presented the mathematical formulation for the hydrodynamics of ferrofluid. Also, he numerically studied the problem of deformation of a ferrofluid droplet

* Corresponding author, e-mail: mnazari@shahroodut.ac.ir; mohsen.naz66@gmail.com

in a uniform magnetic field by coupling the magnetic field, the free surface, and the fluid--flow. Flament *et al.* [11] experimentally investigated the equilibrium shape of a ferrofluid droplet in a uniform magnetic field in a Hele-Shaw cell. They observed the droplet is elongated in the direction of the magnetic field.

In the past decade, a number of techniques have been developed to simulate deformation droplet or bubble under magnetic field by invoking traditional computational methods such as volume of fluid (VOF) [12, 13] method, level set (LS) [14, 15] method, and front tracking method. The simulation of complex two-phase flow is an interesting and challenging problem because of the intrinsic problem in tracking the moving interface like applying surface tension and conservation of mass appropriately. Also, the behavior of the interface in ferrofluids is completely different from that of common liquids due to sudden changes at magnetic properties of ferrofluids. Recently, the lattice Boltzmann method (LBM) has emerged as a promising alternative technique for fluid-flow simulations such as natural convection [16-18], nanofluid [18-21], unsteady flow [22, 23], non-Newtonian flow [24, 25], multiphase flow [26, 27], and so on. The LBM based immiscible multiphase flow model can be divided into four distinctly different LBM approaches: the chromo-dynamic model [28], pseudo-potential model [29] (also known as the Shan-Chen), the intermolecular interaction models [30], and the free energy (FE) approach [31]. Among these models, pseudo-potential model is the most famous model due to its simplicity and adaptability. Therefore, we used pseudo-potential model to study the effect of uniform magnetic field on falling and the coalescence of a pair ferrofluid droplets.

To the author best knowledge, simulation of falling and the coalescence of a pair ferrofluid droplets subjected to uniform magnetic field is not studied yet. This paper reports the development of a robust 2-D numerical code to simulate falling and the coalescence of a pair ferrofluid droplets subjected to uniform magnetic field. To this approach, a hybrid lattice--Boltzmann with Shan-Chen model and finite-volume method is implemented. The LBM was used to track the moving interface between two immiscible phases and update the flow field by adding magnetic field force in lattice Baltzmann equations while the magnetic induction equation is solved using the finite volume method to calculate the magnetic field. The effects of the magnetic Bond number, susceptibility, and magnetic field direction on a deformation of the falling droplet are investigated in details

Mathematical formulations

Shan-Chen interparticle potential LBE model

In this study, the multi-component LBM proposed by Shan and Chen [32] is applied to simulate ferrofluid droplet falling in the vertical channel. The distribution functions of the lattice Boltzmann equation using the single relaxation time collision for multiphase flow are [33]:

$$f_i^\sigma(\boldsymbol{x},\boldsymbol{e}_i\delta t,t+\delta t)=f_i^\sigma(\boldsymbol{x},t)-\frac{1}{\tau^\sigma}[f_i^{\sigma(\mathrm{eq})}(\boldsymbol{x},t)-f_i^\sigma(\boldsymbol{x},t)] \tag{1}$$

where, f_i is the particle distribution function of component σ along the i^{th} direction, δt – the time step size, and f^{eq} – the equilibrium distributions function of f, and given by [23]:

$$f_i^{\sigma(eq)} = w_i \rho^\sigma \left(\boldsymbol{x}, t\right) \left[1 + \frac{\boldsymbol{e}_i \boldsymbol{u}_{\boldsymbol{eq}}^\sigma}{c_s^2} + \frac{1}{2} \frac{(\boldsymbol{e}_i \boldsymbol{u}_{\boldsymbol{eq}}^\sigma)^2}{c_s^4} - \frac{1}{2} \frac{\boldsymbol{u}_{\boldsymbol{eq}}^{\sigma\,2}}{c_s^2} \right] \tag{2}$$

where $\boldsymbol{e}_i$ denotes the particle velocity in the i^{th} direction. Lattice models are usually described as D_nQ_m, where n is the dimension and m is number of i directions. In this simulation, D_2Q_9 is used. Hence, the particle velocity is defined [23]:

$$\begin{gathered} e_0 = (0,0), \\ e_{1,3}, e_{2,4} = (\pm c, 0), \quad (0, \pm c), \\ e_{5,6,7,8} = (\pm c, 0), \quad (0, \pm c) \end{gathered} \tag{3}$$

where, w_i are weighting factors for each velocity (w_0= 4/9, w_i= 1/9 for i = 1-4, and w_i= 1/36 for i = 5–8). The macroscopic density, ρ, and velocity, $\boldsymbol{u}$, in the lattice unit for each component are obtained from:

$$\rho^\sigma = \sum_{i=0}^{8} f_i^\sigma \tag{4}$$

$$\boldsymbol{u}^\sigma = \sum_{i=0}^{8} \frac{\boldsymbol{e}_i f_i^\sigma}{\rho^\sigma} \tag{5}$$

In the multicomponent model for each component, $\boldsymbol{u}_{eq}^\sigma$, appearing in eq. (2), is given by [33]:

$$\boldsymbol{u}_{eq}^\sigma = \boldsymbol{u}' + \frac{\boldsymbol{\tau}^\sigma}{\boldsymbol{\rho}^\sigma} \boldsymbol{F}^\sigma \tag{6}$$

where τ^σ is the relaxation time of component σ and relates to kinematic viscosity $\mu^\sigma = (\tau^\sigma - 0.5) c_s^2 \delta t$. Also, $\boldsymbol{u}'$ is velocity common to the various components defined:

$$\boldsymbol{u}' = \frac{\displaystyle\sum_{\sigma=1}^{2} \frac{\boldsymbol{\rho}^\sigma \boldsymbol{u}^\sigma}{\boldsymbol{\tau}^\sigma}}{\displaystyle\sum_{\sigma=1}^{2} \frac{\boldsymbol{\rho}^\sigma}{\boldsymbol{\tau}^\sigma}} \tag{7}$$

where $\boldsymbol{F}^\sigma$ is the total interaction force exerted on the σ^{th} component expressed as including fluid-fluid interaction, $\boldsymbol{F}_{\text{f}}^\sigma$, fluid-solid interaction, $\boldsymbol{F}_{\text{s}}^\sigma$, gravity force, $\boldsymbol{F}_a^\sigma$, and magnetic force, $\boldsymbol{F}_{\text{mag}}^\sigma$ [33]:

$$\boldsymbol{F}^\sigma = \boldsymbol{F}_{\text{f}}^\sigma + \boldsymbol{F}_{\text{s}}^\sigma + \boldsymbol{F}_g^\sigma + \boldsymbol{F}_{\text{mag}}^\sigma \tag{8}$$

where $\boldsymbol{F}_{\text{f}}^\sigma$, is the fluid-fluid interactive force proposed by Shan and Chen [32]. The fluid-fluid interaction force can be given by [33]:

$$\boldsymbol{F}_f^\sigma(\boldsymbol{x}) = -\psi^\sigma(\boldsymbol{x}) \sum_{\boldsymbol{\sigma}=1}^{2} G_{\boldsymbol{\sigma}\bar{\boldsymbol{\sigma}}} \sum_{i=0}^{8} w_i \psi^{\bar{\sigma}}(\boldsymbol{x} + \boldsymbol{e}_i \delta t) \boldsymbol{e}_i \tag{9}$$

where $G_{\sigma\bar{\sigma}}$ is the interaction strength between two components σ and $\bar{\sigma}$, ψ^{σ} – the interparticle potential of components σ and $\bar{\sigma}$. Several functional forms of ψ^{σ} have been proposed and the interaction force is calculated from the interaction potential to induce proper phase separation. In the current simulation work, the first component is assumed to be a non-ideal fluid whose potential can be expressed by:

$$\psi^{\sigma} = \rho_0 \left[1 - \exp\left(-\frac{\rho^{\sigma}}{\rho_0} \right) \right] \tag{10}$$

and the second component is assumed to be an ideal fluid which has no interaction in itself, but it interacts with the other component:

$$\psi^{\sigma} = \rho^{\sigma} \tag{11}$$

where $\boldsymbol{F}_{\mathrm{s}}^{\sigma}$ is the fluid-solid interactive force. Similarly, the fluid-solid interaction force is calculated by [33]:

$$\boldsymbol{F}_{\mathrm{s}}^{\sigma}(x) = -\psi^{\sigma}(x) \sum_{i=0}^{8} w_i G_{\sigma w} s(\boldsymbol{x} + \boldsymbol{e}_i \delta t) \boldsymbol{e}_i \tag{12}$$

where s is a switch function that equals zero for fluid nodes and unit for solid nodes. The $G_{\sigma w}$ is the interaction strength between solid and fluid component σ. In the pseudopotential model, wetting conditions on the solid boundary can be easily implemented by relative strength of G_{1w} and G_{2w}. When $G_{1w} - G_{2w} < 0$, of first component is modeled as the wetting phase and the second component is the non-wetting phase. And $\boldsymbol{F}_{\mathrm{mag}}^{\sigma}$ is the magnetic force that will be described in the next section.

Magnetic field governing equations

The magnetic field is described by the magnetostatic Maxwell's equations for a non--conducting ferrofluid. The equations of Maxwell for non-conducting fluids are [34]:

$$\nabla \times \mathbf{H} = 0 \tag{13}$$

$$\nabla . \mathbf{B} = 0 \tag{14}$$

where **H** and **B** are the magnetic field and the magnetic induction, respectively. We consider a ferrofluid domain, Ω_{d} surrounded by a non-magnetic medium, Ω_c, and the **B** satisfies the following [34].

$$\mathbf{B} = \begin{cases} \mu_0 (\mathbf{H} + \mathbf{M}) & \text{if } \Omega_d \\ \mu_0 H & \text{if } \Omega_c \end{cases} \tag{15}$$

where $\mu_0 = 4\pi \cdot 10^{-7}$ N/A^2 is the permeability constant of free space. **M** denotes magnetization of the ferrofluid. Assuming the ferrofluid to be a linear function of the magnetic field [34]:

$$\mathbf{M} = \chi \mathbf{H} \tag{16}$$

where χ is the susceptibility. The magnetic permeability of the ferrofluid is defined as $\mu = \mu(1 + \chi)$. Thus, the magnetic induction inside the ferrofluid is $\mathbf{B} = \varLambda\mathbf{H}$. The magnetic field is determined in the form of $\mathbf{H} = -\nabla \varnothing$ (where $\varnothing$ is scalar potential). By combining eqs.

(13), (14) and using $\mathbf{H} = -\nabla\varnothing,$ the magnetic field equation governing the problem can be stated [34]:

$$\nabla\left[\Lambda\nabla\varnothing\right] = 0 \tag{17}$$

where μ varies sharply at the interface. As a result, the scalar potential changes as the interface is moving. Then, the magnetic permeability can be expressed [35]:

$$\Lambda_\varepsilon(\varnothing) = \Lambda_\mathrm{d} H_\varepsilon(\varnothing) + \Lambda_\mathrm{c}[1 - H_\varepsilon(\varnothing)] \tag{18}$$

where the subscripts c and d refer to the continuous and dispersed phases, respectively, and $H_\varepsilon(\emptyset)$ is the modified Heaviside function and is defined:

$$H_\varepsilon(\zeta) = \begin{cases} 0 & \text{if } \rho = \rho_1 \\ \dfrac{1}{2}[1 + \zeta + \dfrac{1}{\pi}\sin(\pi\,\zeta) & \text{if } \rho_1 < \rho < \rho_2 \\ 1 & \text{if } \rho = \rho_2 \end{cases} \tag{19}$$

where ζ is a parameter defined:

$$\zeta = \frac{\rho_1}{\rho_1 + \rho_2} \tag{20}$$

Modeling of applied magnetic field effect

The effect of magnetic field on flow field is considered by adding magnetic force to Lattice Boltzmann equation. The force acting on a linearly magnetizable ferrofluid in the isothermal system is expressed by Rosensweing [10]:

$$\boldsymbol{F}_\mathrm{mag} = -\frac{1}{2}H^2\nabla\Lambda \tag{21}$$

The magnetic force can be rewritten by substituting eq. (18) into eq. (21) [10]:

$$\boldsymbol{F}_\mathrm{mag} = -\frac{1}{2}H^2(\Lambda_\mathrm{c} - \Lambda_\mathrm{d})\delta_\varepsilon(\zeta)\nabla\zeta \tag{22}$$

The modified smoothed delta function is defined:

$$\delta_\varepsilon(\zeta) = \frac{\partial \mathrm{H}_\varepsilon(\zeta)}{\partial\zeta} = \begin{cases} 0 & \text{if } \rho_1 = \rho \text{ or } \rho = \rho_2 \\ \dfrac{1}{2}[1 + \cos(\pi\zeta)] & \text{if } \rho_1 < \rho < \rho_2 \end{cases} \tag{23}$$

Problem description

Figure 1 shows the flow geometry and computational domain. At the initial time, the initial shape of ferrofluid droplets is assumed to be spherical and released in a stationary non-magnetic fluid, which falls driven by the gravity. The initial distance between the centers of the droplets is considered to be two times of the droplets' initial diameter. Bounce-back boundary condition is employed at the side walls and periodic boundary condition is applied at the up and down boundaries in flow field. To avoid the wall effect on droplet shape, the

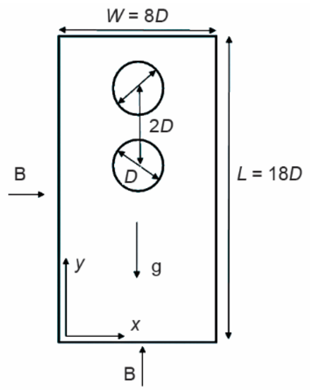

Figure 1. Schematic geometry of problem

ratio of the width of the domain, W, to the droplet diameter, D, is chosen 8 in all next simulations. Also, the minimum channel height, L, must be sized so that the falling droplet can be reached steady-state which in this research is eighteen times the initial drop diameter. In order to obtain magnetic field, the magnetic potential should be initially calculated by numerically solving eq. (17). The governing equations are discretized by the finite volume method in a 2-D Cartesian co-ordinate. The spatial discretization of the governing equations is conducted on a uniform grid in a 2-D Cartesian co-ordinate by the finite volume method. The magnetic potential eq. (16) is discretized using second-order central difference and solved by using the ADI method. The magnetic scalar potential boundary condition under vertical and horizontal magnetic field is applied, respectively:

$$\text{Horizontal}: \begin{cases} \dfrac{\partial \phi}{\partial y} = 0 & \text{Top and bottom} \\ \Lambda_0 H_0 = \Lambda_2 \dfrac{\partial \phi}{\partial x} & \text{Right and left} \end{cases} \tag{24}$$

$$\text{Vertical}: \begin{cases} \Lambda_0 H_0 = \Lambda_2 \dfrac{\partial \phi}{\partial y} & \text{Top and bottom} \\ \dfrac{\partial \phi}{\partial x} = 0 & \text{Right and left} \end{cases} \tag{25}$$

In the case of the deformation and interaction of a pair of co-axial ferrofluid droplets falling in a nonmagnetic liquid under a uniform magnetic field, surface tension between the fluids, viscosity of fluids, initial diameter of the droplets, distance between droplets, density of fluids, magnetic field intensity and susceptibility are the main parameters. In order to non--dimensionalize the parameters, the following dimensionless numbers are introduced:

$$\text{Eo} = \frac{\text{g}\Delta\rho D^2}{\gamma}, \quad \text{Oh} = \frac{\eta_\text{c}}{\gamma D \rho_\text{c}}, \quad \text{Bo}_\text{m} = \frac{\Lambda_0 D H^2}{\gamma}, \quad \chi = \frac{\Lambda_\text{d}}{\Lambda_\text{c}} - 1 \tag{26}$$

where ρ, η, Eo, Oh, Bo_m, and χ are density, viscosity, Eotvos number, Ohnesorge number, magnetic Bond number and susceptibility, respectively, g, γ , $\Delta\rho$, Λ, and H are gravitational acceleration, surface tension coefficient, density difference of the two phases, magnetic permeability, and magnetic field, respectively. Also, subscripts c and d refer to the continuous and dispersed phases, respectively.

Model validation

In order to verify present method, three test cases have been considered: Laplace law, multiple rising bubbles and deformation of static drop under the magnetic field is also simulated.

Laplace law

In order to verify the Laplace law, a droplet with different diameters is located in the center of the computational domain. The interfacial tension was evaluated based on the following analytical relation:

$$\Delta P = \frac{\gamma}{R} \tag{27}$$

where γ, R and ΔP are a surface tension coefficient, droplet radius, and the pressure difference between the inside and the outside of the drop, respectively. In order to the simulation of this problem, a grid with the size of $L \times L$ lattice units and periodic boundary conditions at all around the computational domain are used. Figure 2 illustrates the change of pressure between the inside and outside of the droplet with the inverse of droplet radius. The surface tension is calculated as the slope of the dependence of ΔP on $1/R$. To obtain the mesh independent solution, the mesh number varied in the x- and y-directions. As can be seen from this figure, it presents a good agreement with the Laplace's law. The linear relationship between ΔP and the inverse of the bubble radius confirms a constant value of the surface tension. The surface tension coefficient for different mesh sizes, 120 × 120, 160 × 160, 200 × 200, and 240 × 240 are 0.07, 0.065, 0.061, and 0.06, respectively, in lattice Boltzmann unit. It can be concluded that surface tension coefficient is constant for mesh size smaller than 200 × 200. Hence, the surface tension coefficient is considered about 0.061 lattice units. In the Shan-Chen model [29], γ is determined by the interaction strength $G_{\sigma\bar{\sigma}}$. In this paper, we select $G_{11} = 0$, $G_{22} = -1.0$, $G_{12} = G_{21} = -0.3$ (with 1 denoting the disperse phase and 2 denoting the continuous phase).

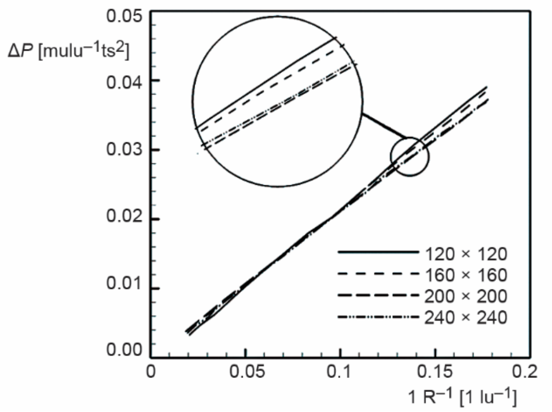

Figure 2. Pressure difference as a function of inverse drop radius (*lu*, *ts*, and *mu* are the length, time, and the mass scales in lattice unit, respectively)

Multiple rising bubbles

In order to validate the flow field, the rising of two co-axial bubbles with initially spherical shapes was simulated. Figure 3 compares our results with results of Delnoij *et al.* [1]. The comparison indicates that the results have good agreement with numerical data.

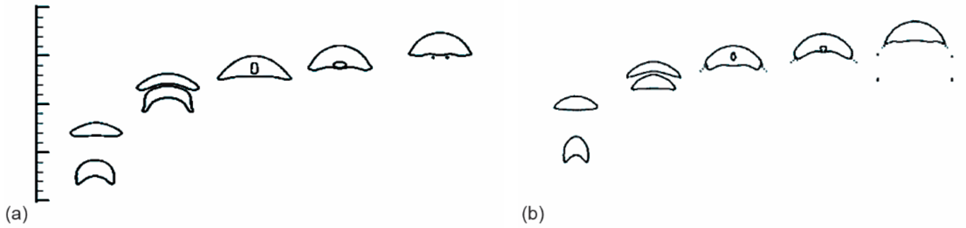

Figure 3. Rising two co-axial bubbles; (a) present study, and (b) Delnoij *et al.* [1] result

Deformation of static drop under magnetic field

To ensure the accuracy of our method, a new simulation is conducted to calculate the equilibrium shape of a ferrofluid droplet within a uniform magnetic field and obtained results are compared with the experimental results of Flament *et al.* [11]. In our test, a stationary circular ferrofluid droplet with radius R is located at the center of a domain of $8R \times 8R$. The permeability ratio of two media is assumed constant as $\Lambda_d / \Lambda_0 = 3.2$. In this case, the gravity is not considered and an external uniform magnetic field is implemented from the bottom to the top. Figure 4 shows the comparison between experimental and numerical results of the droplet shape at the different Bo_m numbers. The magnetic Bond number is the ratio of the magnetic force to the surface tension force. As expected, the drop is elongated along the direction of the uniform magnetic field until it reaches the stable equilibrium shape.

In order to examine the accuracy of the current hybrid-algorithm quantitatively, the values of aspect ratio, b/a, at the equilibrium state of ferrofluid droplets for different susceptibilities at $Bo_m = 2.13$ were compared by the numerical results of Ghaffari *et al.* [36] in fig. 5, b is the major axis and a is the minor axis. As shown in this figure, there is a good agreement between the present simulation and the results obtained by Ghaffari *et al.* [36].

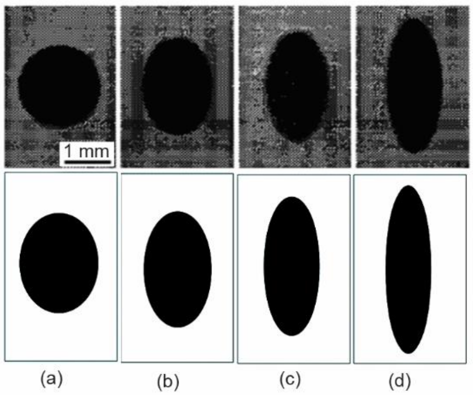

Figure 4. Comparison of equilibrium droplet shapes observed in experiments [11] (top row) with that predicted by simulation (bottom row); (a) $Bo_m = 0.6$, (b) $Bo_m = 2.4$, (c) $Bo_m = 3.5$, and (d) $Bo_m = 5.7$

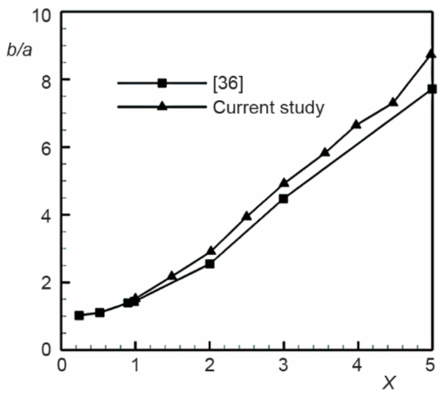

Figure 5. A comparison between current study and numerical study of Ghaffari *et al.* [36] for the values of aspect ratio, *b*/*a*, at the equilibrium state of ferrofluid droplets for different susceptibility at $Bo_m = 2.13$

Result and discussion

Falling and the coalescence of a pair of ferrofluid droplets in a magnetic field in which their initial centers located on a vertical line highly depend on the magnetic field as well as the flow field. The magnetic Bond number, Bo_m, and the susceptibility, χ, are used to represent the influence of magnetic field on droplets deformation and the coalescence. Figure 6 illustrates the magnetic field lines around the falling droplets at different dimensionless times, $t^* = t/(D/g)^{0.5}$, under vertical magnetic field with the flow conditions of Oh = 0.15; $Oh = \mu_c/(\sigma D \rho_c)$, Eo = 0.5, $Bo_m = 2.4$, and $\mu_d/\mu_c = 2$. It is evident that the uniform magnetic field lines distort across the interface due to the permeability changes in value and they are identical inside or far away from the droplet. In fact, the materials with low magnetic permeability show higher resistance against the applied magnetic field in contrast with those have high magnetic permeability. As a result of this, the magnetic field lines tend to pass through the droplet due to the permeability of ferrofluid droplet which is higher than that of surrounding phase. Hence, the concentration of the magnetic field lines inside the droplet is greater than that of the other phase due to the higher permeability of a ferrofluid droplet with respect to non-magnetic viscous fluid. Therefore, the effect of magnetic field strength inside the droplet is stronger than the magnetic field outside the droplet, and the direction of the net force is toward the outside of the droplet.

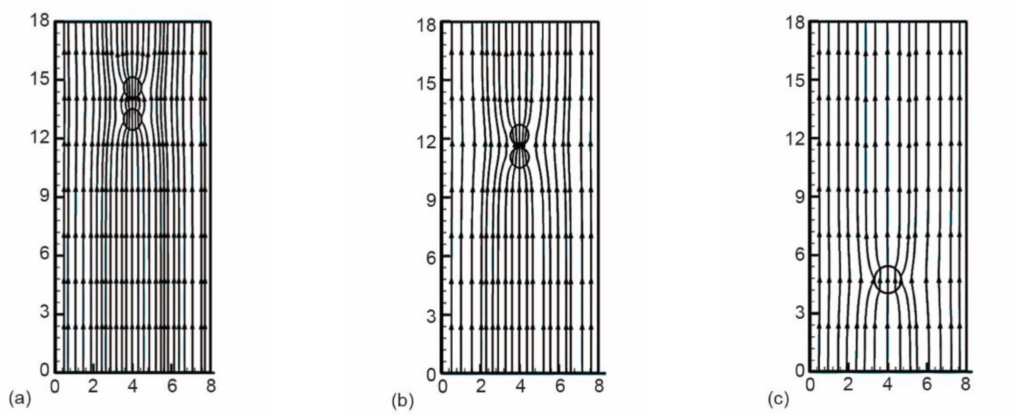

Figure 6. Magnetic field line for Eo = 0.5, Oh = 0.15, χ = 2, and Bo$_m$ = 2.4, at different t^*; (a) t^* = 3, (b) t^* = 5, (c) t^* = 10

Figure 7 presents the effect of magnetic fields with on a pair of ferrofluid droplets falling in non-magnetic liquid. The figure also compares this condition with the case of no--magnetic field effect at different time instants of the droplets falling under the flow conditions of Oh = 0.15, Eo = 0.5 and χ = 3 for four different magnetic Bond numbers (Bo$_m$= 0, 2.4, 5.4, and 9). The first column of fig. 7 shows the falling and the interaction of a pair of droplets on a vertical line in the absence of magnetic field effects. As time goes on, the trailing droplet falls in the wake region of the leading droplet. The falling velocity of the trailing droplet is increased until the distance between the two droplets decreases. Eventually, the trailing droplet reaches to the leading one and two droplets merge into a larger one. It is necessary to mention that if the initial distance between the droplets becomes higher so that the trailing droplet is not affected by the low-pressure zone in the wake of the leading droplet, two droplets do not collide with each other. As compared in fig 6, it is found that the distance between the droplets decreases by increasing magnetic Bond number, as a result of this, the coalescence of two droplets occurred faster. Also, applied magnetic field affects on the shape of the droplets before and after the coalescence. In the absence of the magnetic field, the deformation of droplet is counteracted by pressure difference, viscous and surface tension forces. It is clear that the droplet shapes are deformed in the direction of the magnetic field when the droplets are exposed in a magnetic field. Generally, the pressure variations that vary along the drops interfaces make the drops oblate, but the magnetic force tends to stretch the drops along the direction of the magnetic field. With the further increase in Bo$_m$, the deformation of the droplets becomes more significant. In fact, the effect of magnetic force is more important than that of surface tension force by increasing Bo$_m$. Figure 7 also shows that the elongation of droplet leads to the droplet width reduction. As a result of the shape effect, the speed of falling droplet becomes fast.

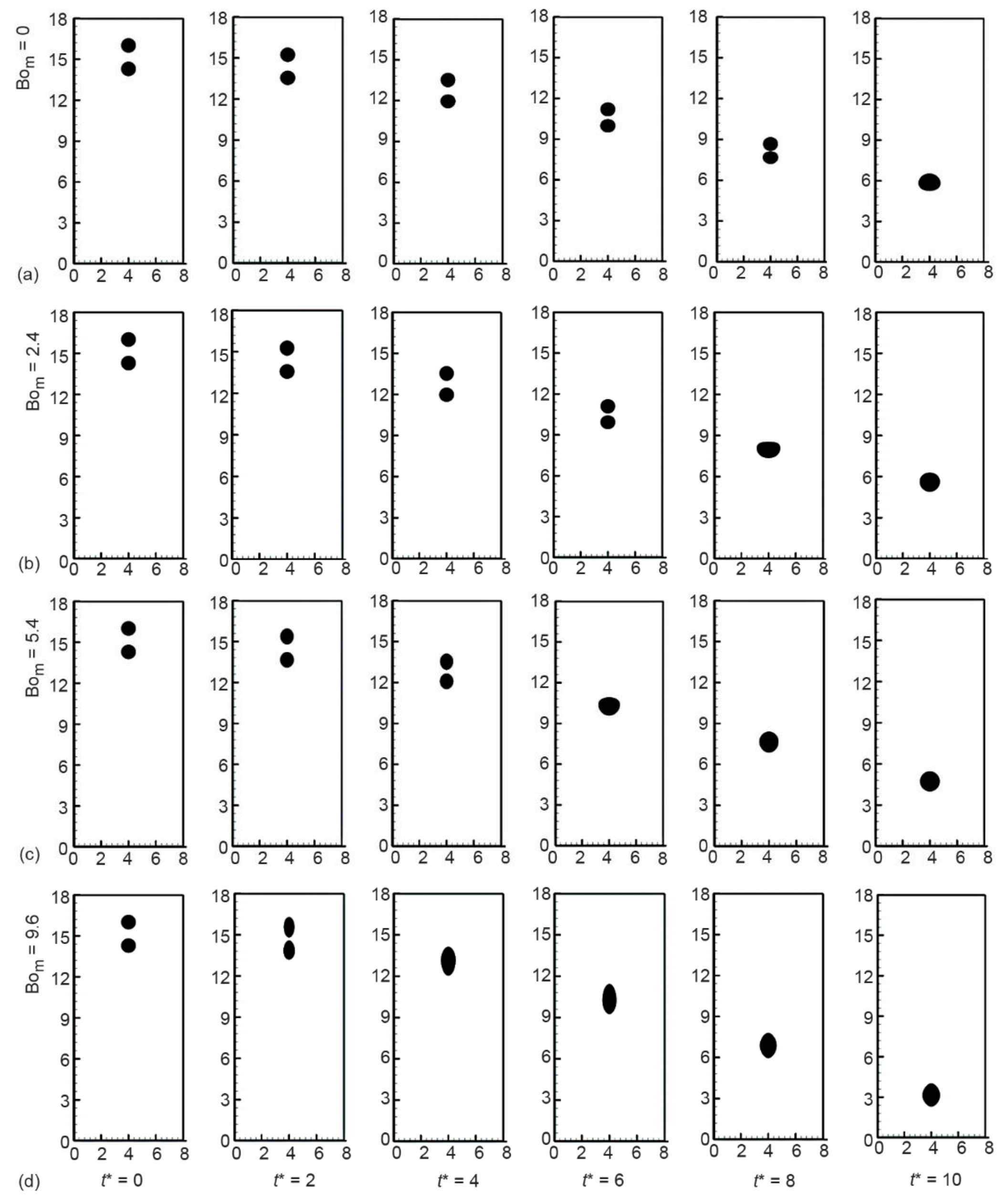

Figure 7. Evolution of the droplet shape for Eo = 0.5, Oh = 0.15, χ = 3, for different Bo_m

Magnetic susceptibility indicates the degree of magnetization of a material in response to an applied magnetic field. In fact, magnetic susceptibility is a quantitative measure of the capability of a material to be magnetized. As mentioned before, there is a direct dependence between the magnetic force imposed on a ferrofluid droplet and magnetic susceptibility. In order to investigate the effect of this parameter, deformation of falling a pair of ferrofluid droplets is illustrated in fig. 8 whereas Eo = 3, Oh_d = 0.1, and Bo_m = 5.4 are consid-

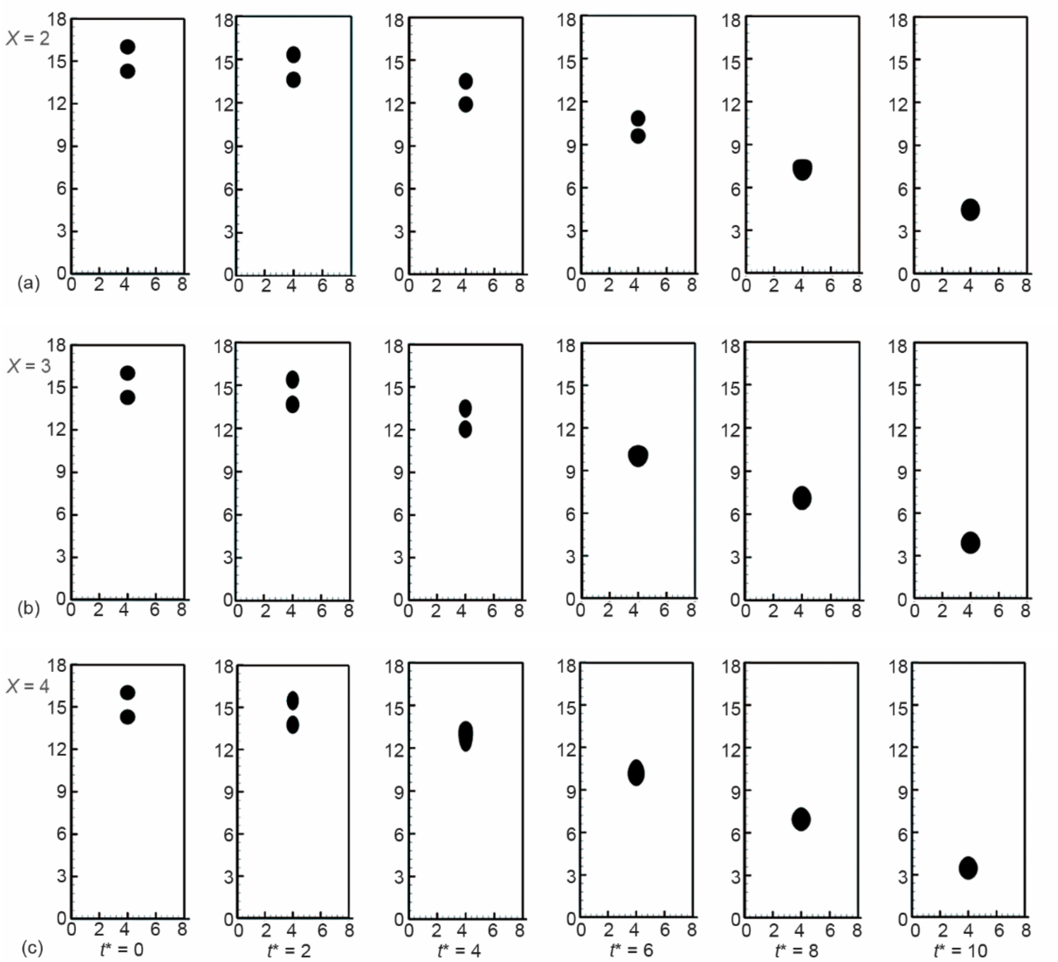

Figure 8. Evolution of droplet shape at different χ under horizontal magnetic field

ered constant. Simulations are performed for different values of susceptibility: χ = 2, 3, and 4. By increasing the susceptibility, χ, at a fixed magnetic Bond number, Bo_m, similar effects of magnetic field on the droplet deformation can be seen in this figure. For low value of susceptibility, the terminal shapes of droplets approximately remain round while for higher values of susceptibility, the droplets elongate more in the magnetic field direction. As the droplets elongate in the vertical direction, the trailing droplet accelerates more and rises fast, therefore, the coalescence occurred more rapidly. To further expand on that, the variation of the time, which last from the droplets falling from a stationary state until coalescence against the magnetic Bond number at different susceptibilities of y-direction magnetic field is illustrated in fig. 9. The diagram clearly shows that the coalescence of droplets occurred faster with increasing susceptibility at the same magnetic Bond number. Also, the coalescence of droplets accelerates by increasing the magnetic Bond number at fix susceptibility. As can be seen, for the highest Bo_m and susceptibility, the reduction of coalescence time becomes more pronounced.

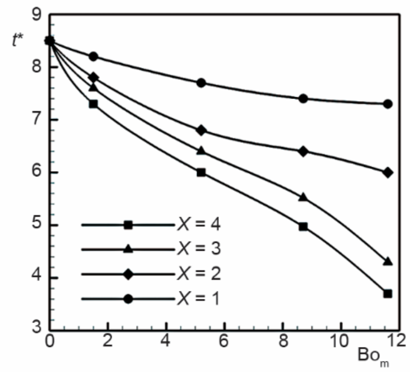

Figure 9. Coalescence time of in-line droplets *vs.* Bo_m at different susceptibility

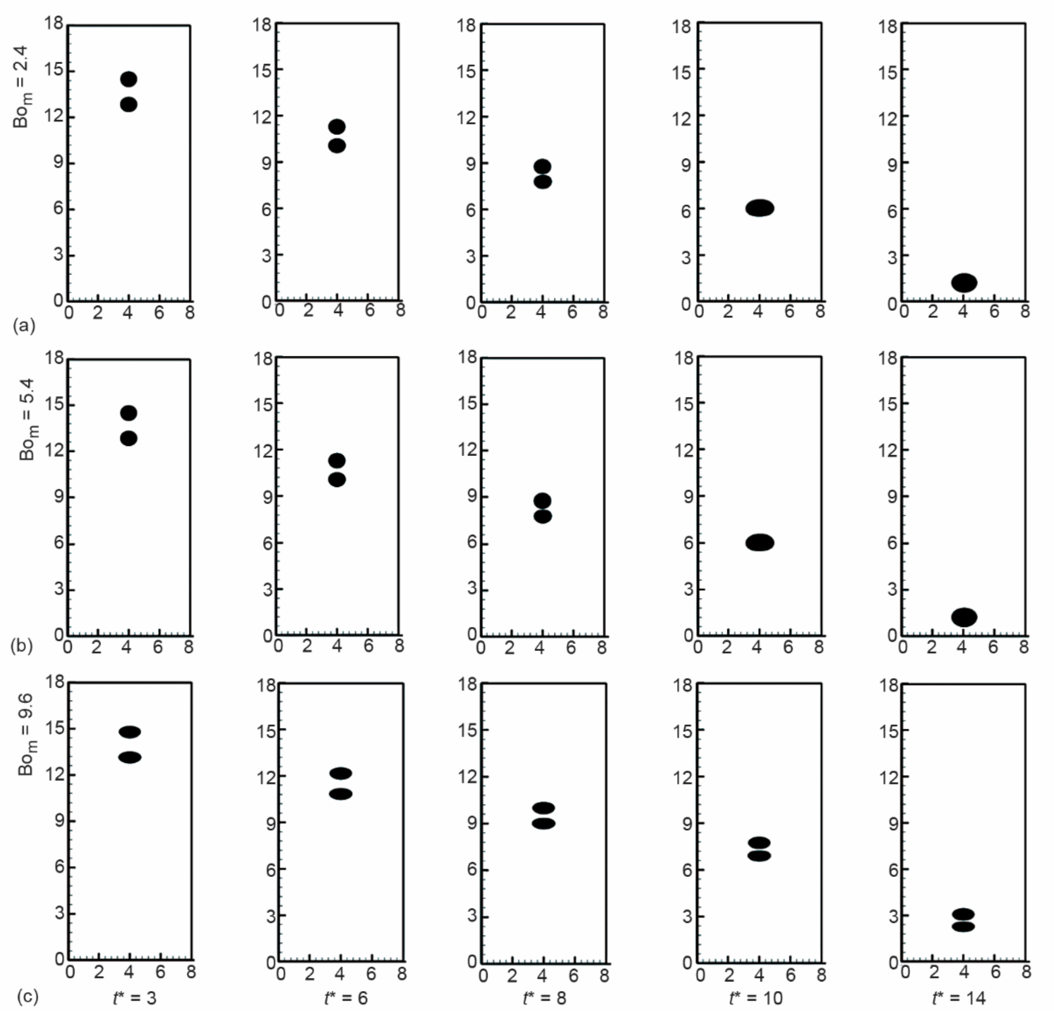

Figure 10. Evolution of droplet shape under horizontal magnetic field for different Bo_m

Figure 10 depicts the effect of the uniform horizontal magnetic field on the falling and the interaction of a pair of droplets in non-magnetic liquid under the flow conditions of Oh = 0.1, Eo = 3, and $\chi = 3$ for three different Bo_m (Bo_m = 2.4, 5.4, and 9.6). As expected, the droplets also elongate in the horizontal direction under the effect of the horizontal magnetic field and the perpendicular area to the droplets motion increases. As a result of the shape effect, the coalescence of droplets postponed as can be seen. In the case Bo_m = 9.6, the coalescence of the droplets is not occurred until t^* = 14. Therefore, the falling process takes more time in the horizontal magnetic field compared to the vertical magnetic field.

According to the figs. 7 and 10, the behavior of a pair of ferrofluid droplets falling in a vertical magnetic field is quite different from that in a horizontal magnetic field. To further expand on that, the spatial co-ordinate of a tip of droplets is presented in fig. 11. This plot compares different cases such as horizontal and vertical magnetic field case with case without magnetic field according to the dimensionless parameters which are demonstrated in fig 9. As can be seen in the fig. 11, the falling process takes more time in the horizontal magnetic field in comparison with the vertical magnetic field.

Figure 12 shows the time histories of surface tension and magnetic field force vectors that act on droplets with a uniform magnetic field in *y*-direction. The obtained vectors are according to the dimensionless parameters demonstrated in fig. 9(c). As it can be seen, these forces act only at the interface. The surface tension force is a function of the local curvature of the interface. The large curvature of the interface leads to an increase in the surface tension force. This surface tension force acts in the opposite direction of the magnetic field force. On the other hand, the direction of the magnetic field force vectors is from inside of droplets to outside of droplets because the magnetic permeability of ferrofluid droplets is higher than nonmagnetic viscous fluid one. By comparison between magnitudes of the vectors on the sides of the droplets, it is found that magnitudes of the vectors on the top and bottom sides of surfaces are greater than left and right one for vertical magnetic fields, so the magnetic force tends to stretch the droplets along the y-direction.

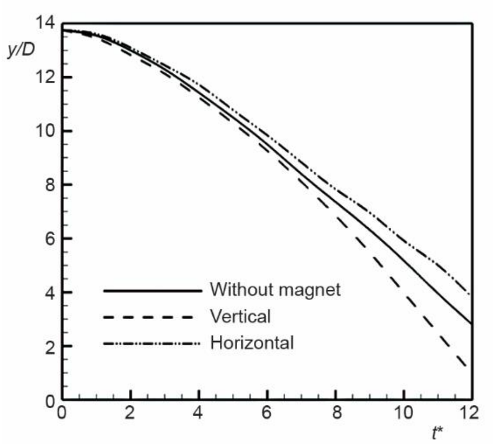

Figure 11. The lowest position of the droplet *vs.* t^* for horizontal, vertical and without magnetic field

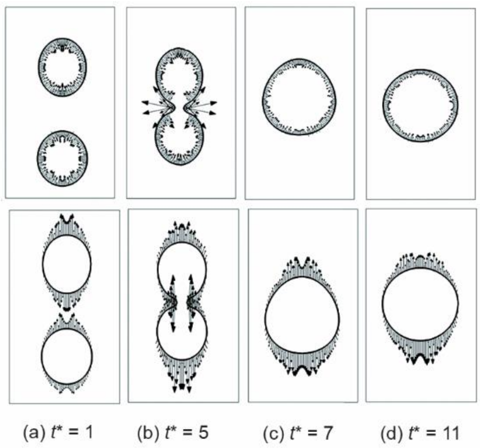

Figure 12. Surface tension force (top row) and magnetic field force (bottom row)

Conclusions

The falling and coalescence of a pair ferrofluid droplet falling in a non-magnetic fluid were simulated using a hybrid Lattice Boltzmann model and finite-volume method. The lattice Boltzmann approach base Shan-Chen model is implemented to track the moving interface between two immiscible phases while the finite volume method is used to solve the magnetic induction equation and calculate the magnetic field. The flow field updates by adding magnetic field force in lattice Boltzmann equations. To validate present method, three test cases are considered: Laplace law, multiple rising bubbles and deformation of static drop under magnetic field.

The comparison of the results shows a good agreement between the results. Then the effects of the magnetic Bond number, susceptibility and magnetic field direction on the coalescence and deformation of droplets were studied in detail. The main results can be summarized as follows.

- The uniform magnetic field lines distort across the interface due to the permeability changes in value and are identical inside and far away from the droplet.
- For vertical magnetic field, the distance between the droplets decreases by increasing magnetic Bond number and susceptibility, and the occurrence of coalescence of two droplets becomes fast.
- The coalescence between droplets and falling process of them decrease by increasing magnetic Bond number and susceptibility for the horizontal magnetic field while a reversed trend is observed for the vertical magnetic field.
- The magnetic field force acts only at the interface and it is zero within both close and far away of the interface. The direction of the magnetic field force vectors is from inside to outside of droplet since the magnetic permeability of ferrofluid is higher than that of nonmagnetic viscous fluid.
- The surface tension force is a function of the local curvature of the interface and it acts only at the interface. Larger curvature of the interface leads to an increase in the surface tension force.
- It is found that a hybrid Lattice Boltzmann base Shan-Chen model and finite-volume method is a reliable and suitable approach for the simulation of falling and coalescence of a pair of ferrofluid droplets under uniform magnetic field.

Nomenclature

a – minor axe, [mm]
b – major axe, [mm]
$\mathbf{B}$ – magnetic induction
Bo_m – Magnetic Bond number [= $(\Lambda_0 DH^2)/\gamma$]
c – lattice speed
c_s – speed of sound
D – droplet diameter, [mm]
Eo – Eotvos number [= $(g\Lambda\rho D^2)/\gamma$]
e – microscopic velocity
$\mathbf{F}$ – external force [kgms^{-2}]
f – distribution function for flow field
f^{eq} – equilibrium distributions function
g – gravity, [ms^{-2}]
$G_{\sigma\bar{\sigma}}$ – interaction strength between two components σ and $\bar{\sigma}$,
$\mathbf{H}$ – magnetic field, [kgs^{-2}A^{-2}]
H_ε – modified Heaviside function
Oh – Ohnesorge number [= $\eta_c/(\gamma D\rho_c)$]
L – height of channel, [mm]
M – magnetization
t – time, [s]
t^* – dimensionless time [= $t/(D/g)^{0.5}$]
u – velocity, [ms^{-1}]
u' – effective velocity, [ms^{-1}]
W – width of the domain, [mm]
w – weighting factor

Greek symbols

ρ – density, [kgm^{-3}]
γ – surface tension coefficient, [Nm^{-1}]
η – viscosity, [kgm^{-1}s^{-1}]
Λ – permeability, [Hm^{-1}]

ψ – interparticle potential
$\varnothing$ – scalar potential
τ – relaxation time
χ – susceptibility
δt – time step size

Subscripts

σ – component
c – continuous phases
d – dispersed phases
f – fuid
s – solid
mag – magnetic

References

[1] Delnoij, E., *et al.* Numerical Simulation of Bubble Coalescence using a Volume of Fluid (VOF) Model, *Proceedings*, 3rd International Conference on Multiphase Flows,Lyon, France, 1998
[2] Guido, S., Simeone, M., Binary Collision of Drops in Simple Shear Flow by Computer Assisted Video Optical Microscopy, *Journal of Fluid Mechanics, 357* (1998), 1, pp. 1-20
[3] Yang, H., *et al.* The Coalescence of Two Equal-Sized Drops in a 2-D Linear Flow, *Physics of Fluids*, *13* (2001), 5, pp. 1087-1106
[4] Ha, J. W., *et al.,* Effect of Compatibilizer on the Coalescence of two Drops in Flow, *Physics of Fluids, 15,* (2003), 4, 849-867
[5] Annaland, M. V. S., *et al.*, Numerical Simulation of Gas Bubbles Behavior using a Three Dimentional Volume of Fluid Method, *Journal of Chemical Engineering Science, 60* (2005), 11, pp. 2999-3011
[6] Yoon, Y., *et al.,* Coalescence of Two Equal-Sized Deformable Drops in an Axisymmetric Flow, *Physics of Fluids, 19* (2007), 10, pp. 102102-1-102102-24
[7] Burns, A., *et al.,* Microfabricated Structures for Integrated DNA, *Proc. Nat. Acad. Sci. U.S.A.*, 93 (1996), 11, pp. 5556-5561
[8] Cordero, M. L., *et al.*, Thermocapillary Manipulation of Droplets using Holographic Beam Shaping: Microfluidic Pin Ball, *Applied Physics Letters, 93* (2008), 3, 034107-1-034107-3
[9] Cho, S. K., *et al.,* Creating, Transporting, Cutting, and Merging Liquid Droplets by Electrowetting-Based Actuation for Digital Microfluidic Circuits., *Journal of Microelectromechanical System, 12*, (2003), 1, pp. 70-80
[10] Rosensweig, R. E., *Ferrohydrodynamics*, Cambridge University Press, Cambridge, UK, 1985
[11] Flament, C., *et al.,* Measurements of Ferrofluid Surface Tension in Confined Geometry, *Journal of Physic Review E, 53* (1996), 5, pp. 4801-4806
[12] Afkhami, S., *et al.*, St: Field Induced Motion of Ferrofluid Droplets Through Immiscible Viscous Media, *Journal of Fluid Mechanics*, *610* (2008), Sept., pp. 363-380
[13] Tian, X. H., *et al.,* Influence of Vertical Static Magnetic Field on Behavior of Rising Single Bubble in a Conductive Fluid, *Journal of Iron and steel Institute of Japan, 56* (2016), 2, pp. 195-204
[14] Kie, H., Level Set Method for Two-Phase Incompressible Flows under Magnetic Fields, *Journal of Computer Physics Communications, 181* (2010), 6, pp. 999-1007
[15] Hadidi, A., Jalali-Vahid, D., Numerical Study of the Uniform Magnetic Field Effect on the Interaction of Bubbles in Viscous Liquid Column, *Theor. Comput. Fluid Dyn. 30* (2016), 3, pp. 165-184
[16] Nazari, M., *et al.,* Lattice Boltzmann Simulation of Natural Convection in an Open End Cavity with Inclined Hot Wall, *Applied Math. and Mech., 36* (2015), 4, pp. 523-540
[17] Nazari, M, *et al.,* Lattice Boltzmann Simulation of Double Diffusive Natural Convection in a Square Cavity with a Hot Square Obstacle, *Chinese Journal of Chemical Engineering*, *23* (2015), 1, pp. 22-30
[18] Ashorynejad, H. R., Hoseinpour, B., Investigation of Different Nanofluids Effect on Entropy Generation on Natural Convection in a Porous Cavity, *European Journal of Mechanics B/Fluids, 62* (2017), Mar.-Apr., pp. 86-93
[19] Fallah, K., *et al.* Simulation of Natural Convection Heat Transfer Using Nanofluid in a Concentric Annulus, *Thermal Science*, *21* (2015), 3, pp. 1275-1286
[20] Alinejad, J., Fallah, K., Taguchi Optimization Approach for Three-Dimensional Nanofluid Natural Convection in a Transformable Enclosure, *Journal of Thermophysics and Heat Transfer, 31* (2016), 1, pp. 211-217
[21] Hoseinpour, B., *et al.* Entropy Generation of Nanofluid in a Porous Cavity by Lattice Boltzmann Method, *Journal of Thermophysics and Heat Transfer, 31* (2017), 1, pp. 20-27
[22] Fallah, K., *et al.,* Numerical Simulation of Planar Shear Flow Passing a Rotating Cylinder at Low Reynolds Numbers, *Acta Mechanica, 223* (2012), 2, pp. 221-236

[23] Fallah, K., *et al,.* Multiple-Relaxation-Time Lattice Boltzmann Simulation of Non-Newtonian Flows past a Rotating Circular Cylinder, *Journal of Non-Newtonian Fluid Mechanics, 177-178* (2012), Jun., pp. 1-14
[24] Amiri Delouei, A., *et al.,* Non-Newtonian Unconfined Flow and Heat Transfer over a Heated Cylinder Using the Direct Forcing Immersed Boundary-Thermal Lattice Boltzmann Method, *Physical Review E (APS), 89* (2014), 5, pp. 053312
[25] Nazari, M., *et al.,* Power-Law Fluid Flow and Heat Transfer in a Channel with a Built-In Porous Square Cylinder: Lattice Boltzmann Simulation, *Journal Non-Newtonian Fluid Mechanics, 204* (2014), Feb., pp. 38-49
[26] Fallah, K., *et al.*, Drop Formation in Cross-Junction Microchannel, using Lattice Boltzmann Method, *Thermal Science, 22* (2016), 2, pp. 909-919
[27] Fallah, K., Taeibi, M., Lattice Boltzmann Simulation of Drop formation in T-junction Microchannel, *Journal of Molecular Liquids, 240,* (2017), Aug., pp. 723-732
[28] Gunstensen, A. K., *et al.,* Lattice Boltzmann Model of Immiscible Fluids, *Journal of Physic Review A, 43* (1991), 8, pp. 4320-4330
[29] Shan, X., Chen, H., Lattice Boltzmann Model for Simulating Flows with Multiple Phases and Components, *Journal of Physic Review E, 47* (1993), 3, pp. 1815-1819
[30] He, X., *et al.*, A Discrete Boltzmann Equation Model for Non-ideal Gases, *Journal of Physic Review E, 57* (1998), 1, doi: http://dx.doi.org/10.1103/PhysRevE.57.R13
[31] Swift, M. R., *et al.*, Lattice Boltzmann Simulation of Nonideal Fluids, *Journal of Physic Review Letters, 75* (1995), 5, pp. 830-840
[32] Shan, X., Chen, H., Lattice Boltzmann Model for Simulating Flows with Multiple Phases and Components, *Journal of Physic Review E, 47* (1993), 3, pp. 1815-1819
[33] Mousavi Tilehboni, S. E., *et al.*, Numerical Simulation of Droplet Detachment from Solid Walls under Gravity Force Using Lattice Boltzmann Method, *Journal of Molecular Liquids, 212* (2015), Dec., pp. 544-556
[34] Afkhami, S., *et al.*, Deformation of a Hydrophobic Ferrofluid Droplet Suspended in a Viscous Medium under Uniform Magnetic Fields, *Journal of Fluid Mechanics, 663* (2010), Nov., pp. 358-384
[35] Ansari, M. R., *et al.*, Effect of a Uniform Magnetic Field on Dielectric Two-phase Bubbly Flows Using the Level Set Method, *Journal of Magmetism and Magnetic Materials, 324* (2012), 23, pp. 4094-4101
[36] Ghaffari, A., *et al.*, CFD Simulation of Equilibrium Shape and Coalescence of Ferrofluid Droplets Subjected to Uniform Magnetic Field, *Colloids and Surfaces A: Physicochemical and Engineering Aspects, 481* (2015), Sep., pp. 186-198

Paper submitted: March 3, 2017
Paper revised: June 8, 2017
Paper accepted: June 26, 2017